Memoirs of the Graduate Schools of Engineering and System Informatics Kobe University
No. 2, pp. 1-7, 2010. doi:10.5047/gseku.e.2010.002

Study of Quantitative Visualization of Sound Field Using a Ripple-Tank

Akira MICHIWAKI[1], Michihisa TSUTAHARA[1],
Kentaro MAE[1], Masaharu MORI[2], Takashi AOYAMA[3]
and Keiichi MURAKAMI[3]

[1]*Graduate School of Engineering, Department of Mechanical Engineering*
[2] *Faculty of Engineering, Department of Mechanical Engineering*
[3] *Numerical Analysis Group, Japan Aerospace Exploration Agency(JAXA)*

(Received October 20, 2010; Accepted January 20, 2011; Online published January 25, 2011)
Keywords: Sound Field, Quantitative Visualization, Ripple-Tank Experiment, Sound Scattering, Water Drop

The ripple-tank experiments have been used for the visualization of the aero-acoustics, but they have been qualitative visualization. The purpose of this research is to obtain quantitative data from the ripple-tank visualization. The optical devices were set up to use the shadowgraph method and the images were digitalized. The Poisson equation governing the wave height, corresponding to the sound pressure, was numerically solved by the finite difference method. In order to examine the validity of the presented technique, a comparison with the theoretical results was conducted on scattering of plane waves by a circular cylinder and a reasonable result was obtained. The ripple tank experiments were shown to be able to estimate the sound field quantitatively.

Introduction

Recent years, the generation mechanism of the sound has been elucidated aiming at the noise reduction. However, the sound field cannot be visualized and an expensive microphone system is necessary to measure the sound field. On the other hand, ripple-tank experiments have been used to obtain the visual information of the two-dimensional acoustic field[1)], but this technique has been qualitative and the quantitative values of the sound pressure have not being obtained. In this paper, a technique will be proposed to determine the sound pressure values quantitatively by numerical calculation based on the image data obtained by the ripple-tank experiment.

1. Experimental technique and device

1.1 Selection of depth of water tank

In order to do the simulation of sound wave by the ripple tank, it is essential to match the characteristics of the water surface waves and the sound waves. In general, the sound waves are non-dispersive but the surface waves are dispersive. When the water depth is adequate, the dispersive feature disappears in surface waves because the effects of the gravity and the surface tension cancel out as described in the book by Lighthill[2)].

In this case, the sound waves can be simulated by the water surface waves and the depth is determined as follows.

Figure 1 shows the coordinate system, where x is taken horizontal direction and the wave propagates in this direction, and z is taken in the vertical direction and η represents the displacement of the wave from the undisturbed surface. For the two-dimensional surface waves, a relationship among the depth h_0, the wave speed (phase velocity) c of the surface wave, and the wave length λ is shown by the following expression[2)],

$$Y = \sqrt{2\pi\left(X + \frac{2\pi}{g\rho_0}\cdot\frac{T}{h_0^2}\cdot\frac{1}{X^2}\right)\tanh\frac{2\pi}{X}} \tag{1}$$

where

$$X = \frac{\lambda}{h_0}, \quad Y = \frac{c}{\sqrt{gh_0}} \tag{2}$$

are non-dimensional wave length and wave speed.

Figure 2 shows the relation between the wave length and the wave speed for variable water depth. The case of water, and the surface tension T=0.074N/m, the density ρ_0=1000kg/m^3, and the gravitational acceleration g=9.8 kg/sec^2 are assumed. This figure shows that the wave speed is almost constant in

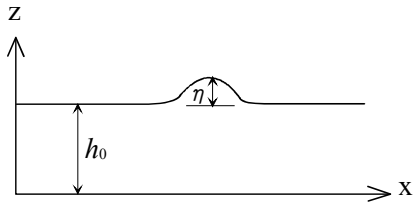

Fig. 1 Coordinate system

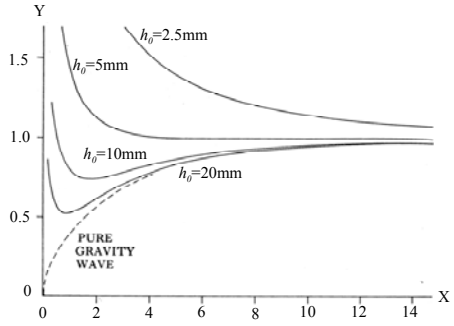

Fig. 2 Relation between water length X and the wave speed Y[2)]

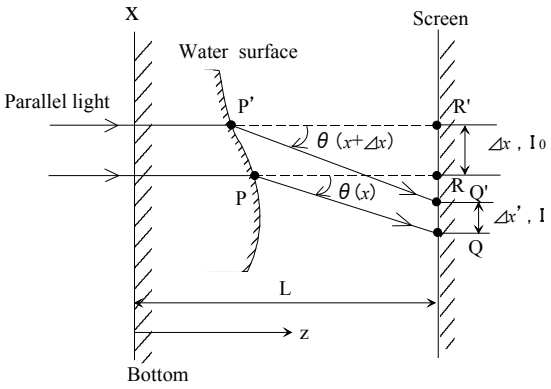

Fig. 3 Path of refracted light

the range of X>4 when the water depth is about 5mm.

1.2 Shadowgraph method for ripple tank

Figure 3 shows the principle of the shadowgraph method. It is assumed that the distance L between the surface of the water and the screen is large. A parallel light goes straight without refracting in the water tank, and the parallel light is refracted by the inclination of the surface of the water. In Fig.3, I_0 represents the brightness in Δx on the screen when going straight without being refracted at the surface of the water, and I represents the brightness in $\Delta x'$ on the screen when refracted at the surface of the water. The relation holds between the two as

$$I_0 \Delta x = I \Delta x' \tag{3}$$

From the geometrical relation

$$\frac{\Delta x'}{\Delta x} = 1 - L\frac{\theta(x+\Delta x)-\theta(x)}{\Delta x} = 1 - L\frac{\partial \theta}{\partial x} \qquad (\Delta x \to 0) \tag{4}$$

Here, in bringing Δx close to 0

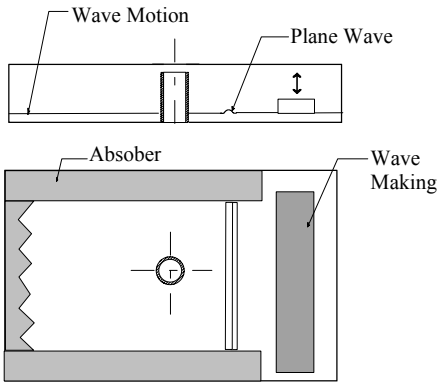

Fig.4 Ripple-Tank

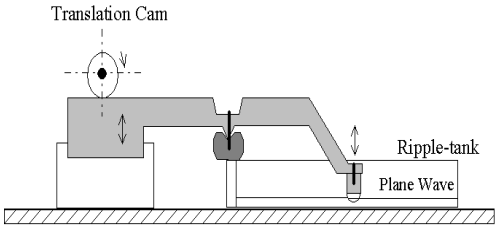

Fig.5 Wave maker

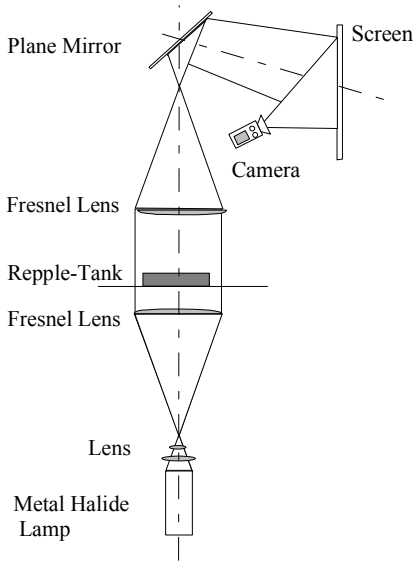

Fig.6 Optical system (Shadowgraph Method)

$$I - I_0 = -(n-1) L I_0 \frac{\partial^2 z}{\partial x^2} \tag{5}$$

where z is the wave height.

When a is assumed to be positive constant, and $\Delta I = I - I_0$, we have

$$\Delta I = -a\frac{\partial^2 z}{\partial x^2} \tag{6}$$

That is, the change in brightness ΔI is proportional to the second order differentiation of height of the wave z.

For two-dimensional case, the y axis is taken in the vertical direction and we obtain

$$\left(\frac{\partial^2 z}{\partial x^2}+\frac{\partial^2 z}{\partial y^2}\right)=-\frac{\Delta I}{a} \tag{7}$$

Solving this Poisson equation, the wave height z is determined.

1.3 Experimental device

Figure 4 shows the ripple-tank system. The water tank was made of acrylic glass of 385mm in length, 276mm in width, and 53mm in height. In order to prevent the reflection of the wave from the walls, the buffer material was arranged. Figure 5 shows the wave maker, in which a circular cylinder was oscillated vertically by using the cam mechanism.

Figure 6 shows the optical system[3]. Metal-halide ramp was used for the source of light. The light becomes parallel through the Fresnel lens of φ600mm, and passes the water layer in the ripple tank. A pattern of bright and dark parts is generated by the refraction due to the difference of the wave height. It is collected with the upper Fresnel lens, and it is projected to a screen.

1.4 Digital processing technique

We took animation pictures of the images with and without the wave. The size of the each image was 640×480Pxls. The animation of each 1 flame was decomposed, and the image was digitalized. Each 1 Pixel shows the brightness value. The difference between the two images was taken by using multifunctional general-purpose image analysis software cosmos32. This processing is effective to exclude the irregularity of the brightness in the background.

1.5 Calculations of wave height

The wave height is obtained by solving the Poisson equation (8). The wave is set to propagate in the x direction. The finite difference method is employed and a uniform square mesh is used, in which 640 in x direction and 480 in y direction. The under relaxation method with the relaxation parameter ω =0.5 is applied in

$$\frac{\partial^2 z}{\partial x^2}+\frac{\partial^2 z}{\partial y^2}+P(x,y)=0 \tag{8}$$

The boundary condition is imposed as follows. The outside boundary in y direction is assumed for the second deferential to be zero.

The direction of y is a Neumann-type boundary condition.

$$\frac{\partial}{\partial x}z(1,y)=\frac{\partial}{\partial x}z(M,y)=0 \tag{9}$$

The convergence condition is.

$$\max\left|\frac{z_{ij}^{(l+1)}-z_{ij}^{(l)}}{z_{ij}^{(l+1)}}\right|<10^{-5} \tag{10}$$

2. Preliminary test of ripple-tank experiment

2.1 Determination of the depth of the water

The experiments were performed for plane waves with the depth 5mm, 10mm and 20mm. The waves move from the left to the right as shown in Fig.7 for the depth 5mm. The height of the surface of the water is shown in Fig.8-10 along the line A-A´ which is the center of the water tank. In these figures, the horizontal axis represents a position of the waves (Pixel) and the vertical axis represents a dimensionless height of the waves based on the maximum height.

A color contour of the plane wave for the depth of 5mm is shown in Fig. 7, and the height of the surface of the water along on A-A´ is shown in Fig. 8. The wave length of the

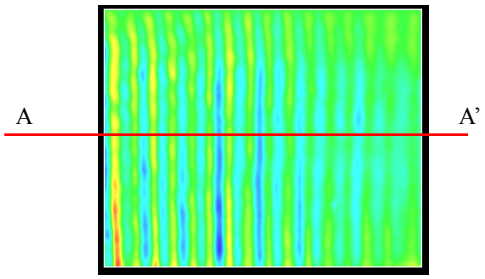

Fig.7 Distribution of plane waves for the depth 5mm

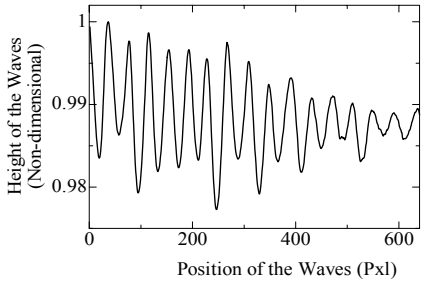

Fig.8 Height of plane waves along the center line A-A' for the depth 5mm

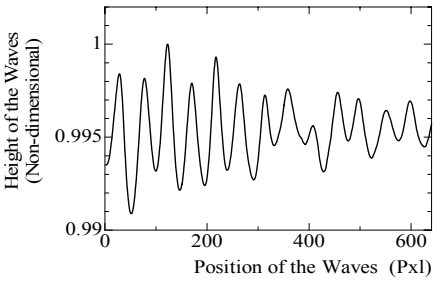

Fig.9 Height of plane waves along the center line for the depth 10mm

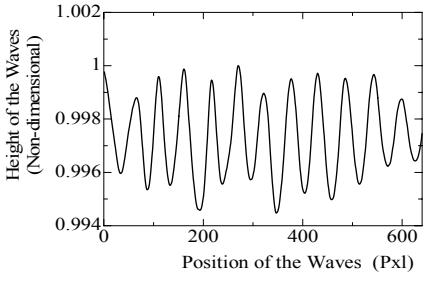

Fig.10 Height of plane waves along the center line for the depth 20mm

plane waves is about 19mm. In this case, it was shown that the plane waves were greatly attenuated. It is thought that this is an effect of the viscosity of water in the boundary layer.

Figure 9 shows the height of the surface of the water along the center line for the depth 10mm. The wave length is about 21mm, and λ/h=2.1. The phase speed of the wave has a dispersion and the shape of waves changes due to the dispersion.

On the other hand, the wave for the depth of 20mm in Fig. 10 shows that the waves do not change their shape nor decrease their height. The variation of the wave height is due to the irregularity of the motion of the wave maker. The wave length is about 23mm and λ/h=1.15. In this condition, we can see the waves do not have the dispersion from Fig.2, and the depth is deep enough to avoid the attenuation due to the boundary layer. We used this condition hereafter.

2.2 Scattering of plane waves by a circular cylinder

2.2.1 Visualization results

Figure 11(a) shows the pattern of plane waves scattered by a circular cylinder with diameter $d = 2\lambda$. Figure 11(b) shows the height of the surface of the water on A-A′ which passes the center of the circular cylinder, and Fig. 11(c) shows the height along the B-B′ which passes the surface of the lower side of the circular cylinder.

2.2.2 Theoretical results

Two-dimensional sound wave equation is solved in wave number domain without the time factor. The incident sound pressure is expressed as, [4)]

$$p_i = P_0 \exp(ikr\cos\theta) = P_0 \varepsilon_n i^n J_n(kr) \tag{11}$$
$$\varepsilon_0 = 1,\ \varepsilon_n = 2\ (n = 1, 2, \cdots)$$

where r is the distance from the center of the circular cylinder and the angle θ is measured from the line in the wave propagation direction, and J_n is the Bessel function. The sound pressure of the scattered wave p_s is expressed in the following form

$$p_s(r,\theta) = \sum_{n=0}^{\infty} C_n \cos n\theta \cdot H_n^{(1)}(\cos\theta) \tag{12}$$

The entire wave field is obtained by assuming the normal differentiation of the pressure on the surface of the cylinder is zero as

$$\sum_n \cos n\theta \left(\varepsilon_n i^n J_n(ka) + C_n H_n^{(1)}(ka) \right) = 0 \tag{13}$$

therefore C_n is determined as

$$C_n = -\frac{\varepsilon_n i^n J_n(ka)}{H_n^{(1)}(ka)} \tag{14}$$

The results are sown in Fig.12(a) where the sound pressure contours are shown and in Figs. 12(b) and 12(c) the sound pressure distributions along A-A' and B-B' are shown respectively.

2.2.3 Comparison between the experimental and theoretical results

The experimental results shown in Fig. 11 are compared with the theoretical results shown in Fig. 12. The wave patterns in Figs. 11(a) and 12(a) are similar and radial interference stripes appeared.

The sound pressure and the wave height shown in Figs.11(b), (c) and Figs.12(b), (c) show that the sound pressure behind the circular cylinder in the experimental results is lower than the theoretical ones. In front of the cylinder, the pressure rises in the theoretical result as shown in Fig. 12(b), but not in the experimental result.

These discrepancies are considered to come from the attenuation of sound scattering at the surface of the cylinder. The theoretical result contains no viscous attenuation, and the decision on which one is realistic can not be done here. In any case, flow visualization technique of the sound field by the ripple-tank is very useful.

3. Simulation of sound pressure reduction effect by a water drop

In order to clarify the mechanism of sound pressure reduction effect by water drops, a simplified experiment was done. A single plane wave was generated and propagated from upper-side to the lower-side as shown in Fig.13. Four kinds of circular cylinders were set on the way. They were solid circular cylinders of aluminum, a sintering metal, a sponge circular cylinder, and soft circular cylinder.

3.1 Effect of outflow from cylinder surface on incidence wave

First, the effect of cylinder surface and the outflow from the surface on the scattering by the cylinder was studied. This outflow corresponds to the evaporation wave, of the water drop. The circular cylinder was made by a porous media, in this case, a sintering metal.

Figure 13 shows the results for the solid and the porous cylinders on the left and center columns and outflow cylinder on the right column in various times. Time t= 0 represents the plane wave front touching the cylinder surface. At this time, some increase of the wave height is observed for solid cylinder, and this is considered to be the capillary effect.

The reflection waves are observed at t= 0.12 sec for all cases. But the reflection by the solid cylinder is the strongest. The weakest reflection by the porous cylinder is due to the inflow and the outflow at the surface of the cylinder. This effect is the same as the deformation of the drop or cylinder. On the other hand, outflow surface generates rather strong reflection wave, As time advances, the reflected waves disappear and transmitted waves through the cylinders remain. The wave for

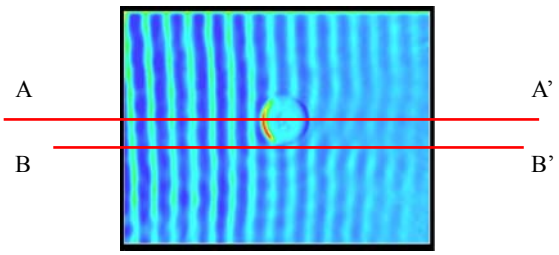

(a) Distribution of plane waves and dispersed waves

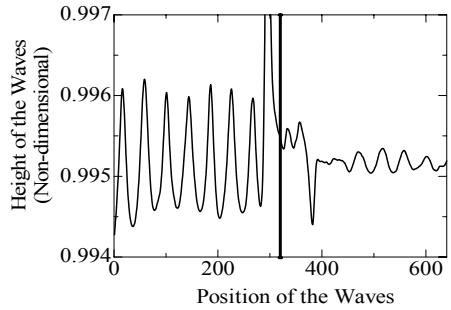

(b) Height of composite waves along the line A-A´

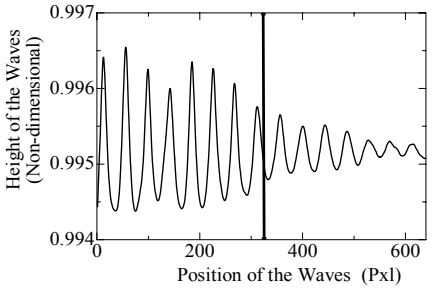

(c) Height of composite waves along the line B-B´

Fig.11 Experimental results

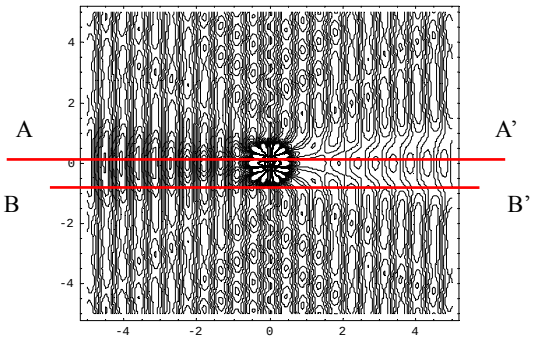

(a) Distribution of plane waves and dispersed waves

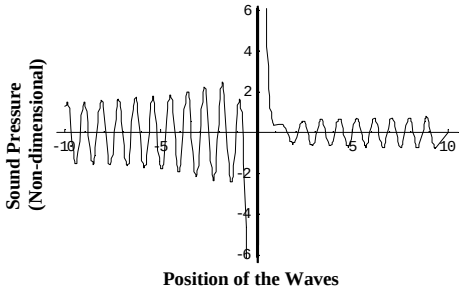

(b) Height of composite waves along the line A-A´

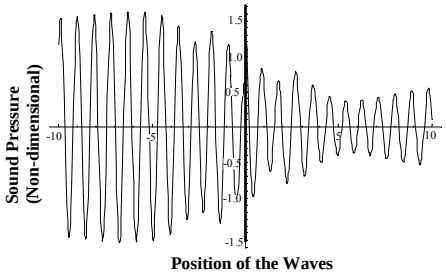

(c) Height of composite waves along the line B-B'

Fig.12 Theoretical results

the solid cylinder is strongest and the others are weaker.

Therefore, the porous surface and outflow surface of the cylinder is effective to reduce the sound pressure when the sound passes through the drop.

3.2 Effect of surface deformation of cylinder on incidence wave

The reduction effect of sound pressure by deformation of the water drop was simulated by using cylinders made of been curd and sponge as the soft material.

The sponge cylinder has two effects, that is the deformation and porous surface effects.

Figure 14 shows the results for solid, sponge and bean curd cylinder. The shape of the reflected wave is not smooth for the bean curd cylinder as shown at t = 0.16 in Fig.14 and this is considered to occur because of the deformation of the cylinder surface. The strengths of reflected waves for three cylinders are almost the same.

The transmitted wave for the solid cylinder is strong and the others are weak, and it is shown that the deformation of the cylinder surface is effective to reduce the sound pressure.

4. Concluding remarks

Quantitative results of sound pressure field by the shadowgraph method using the ripple-tank experiment were obtained. The comparison between the experimental and theoretical results on scattering of the plane wave by a circular cylinder showed good agreement. The effect of reducing the sound pressure by water drops were also studied by this method, and it was shown that the deformation and evaporation of the drop were effective to the sound pressure.

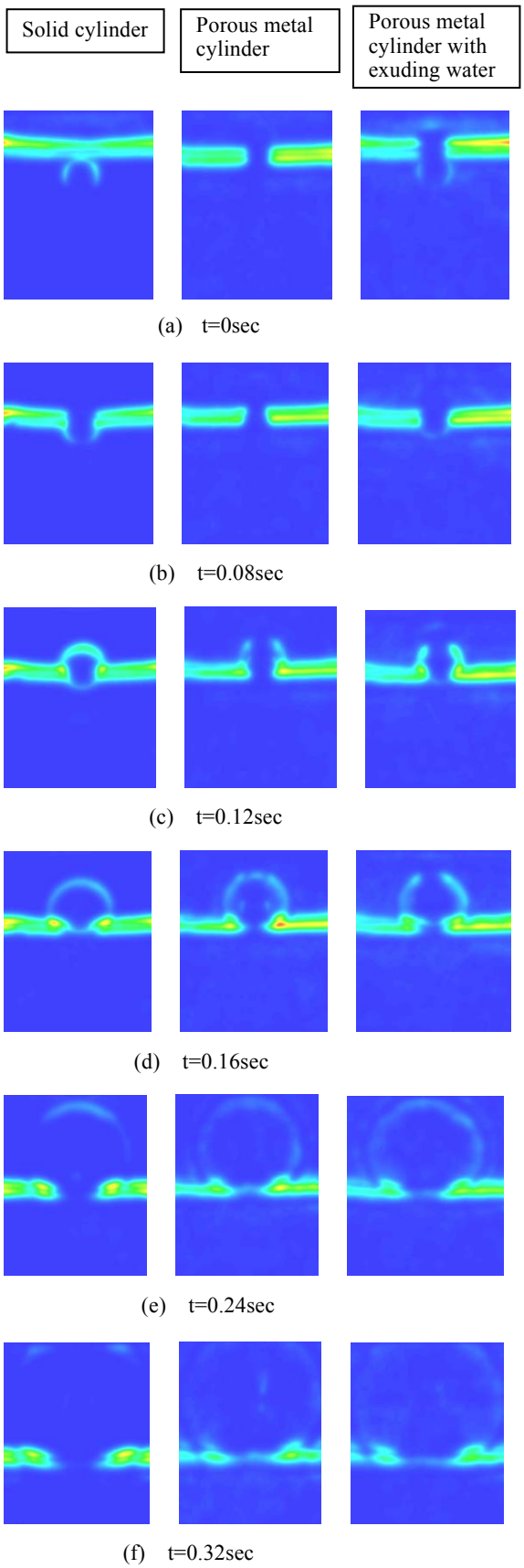

Fig.13 Height of wave coming to one cylinder, The circular cylinder represents from left, rigid cylinder, porous metal cylinder, and porous metal cylinder with exuding water, respectively.

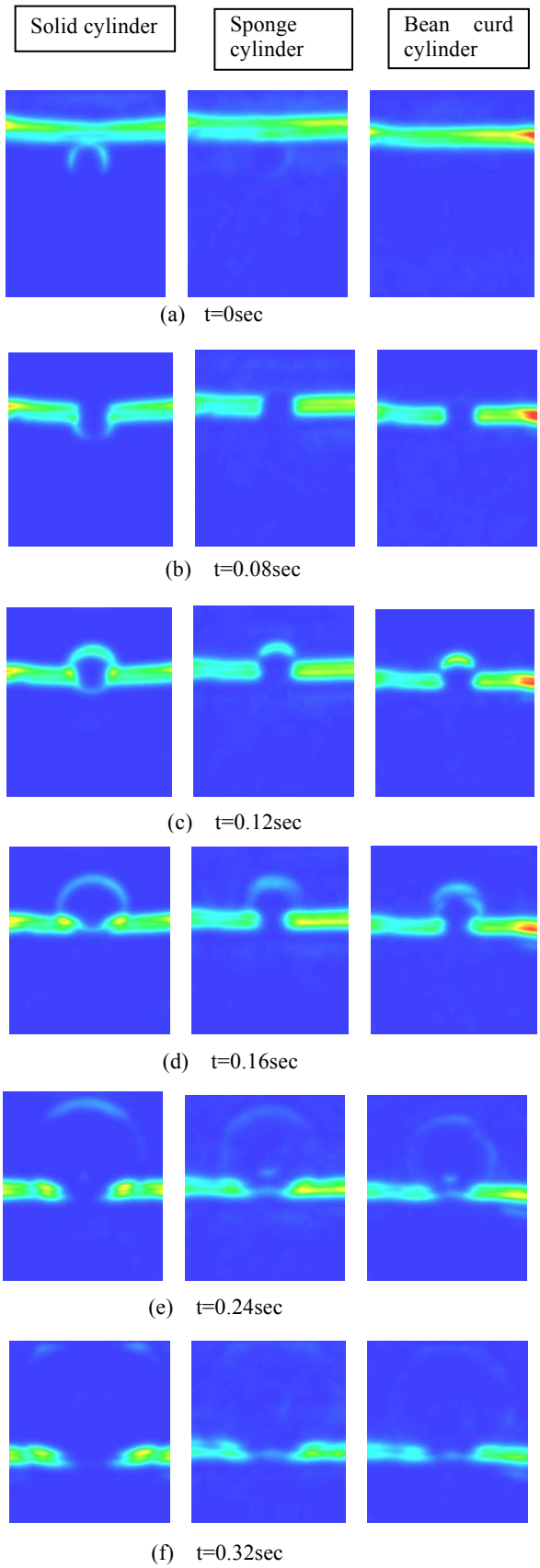

Fig.14 Height of wave coming to one cylinder, The circular cylinder represents from left, rigid cylinder, sponge cylinder, and cylinder of soft material, respectively.

Nomenclature

a = constant in Eq.(6)
c = wave speed [m/s]
C_n = coefficients in Eq.(12)
D = diameter of circular cylinder [m]
h_0 = depth of water [m]
H_n = Hankel function
I_0 = brightness before refraction [cd/m^2]
I = brightness after refraction [cd/m^2]
J_n = Bessel function
L = distance [m]
P_s = sound pressure of scattered wave [Pa]
r = distance from the center of the circular cylinder [m]
X = non-dimensional wave length
Y = non-dimensional wave speed
z = wave height [m]
Δx = distance [m]
$\Delta x'$ = distance [m]
λ = wave length [m]
η = displacement of the wave [m]
θ : = angle from the center of the circular cylinder [rad]

References

1) Wolfgang Merzkirch, "Flow Visualization", Academic Press (1987).
2) James Lighthill M.J, "Waves in fluid", Cambridge University Press (1978).
3) Yoshimichi Tanida et al., "Visualization handbook of flow", Asakura shoten (in Japanes) (1986).
4) Yoshinori Inoue et al., "Nonlinear phenomenon of disorder and wave", Asakura shoten (in Japanes) (1993).